Magnetic symmetries of terbium tetraboride (TbB_4) revealed by resonant x-ray Bragg diffraction

R. D. Johnson [1,2] and S. W. Lovesey [2,3,4]

[1]*Department of Physics and Astronomy, University College London, Gower Street, London WC1E 6BT, England, United Kingdom*
[2]*Diamond Light Source, Harwell Science and Innovation Campus, Didcot, Oxfordshire OX11 0DE, England, United Kingdom*
[3]*ISIS Facility, STFC, Didcot, Oxfordshire OX11 0QX, England, United Kingdom*
[4]*Department of Physics, Oxford University, Oxford OX1 3PU, England, United Kingdom*

(Received 25 June 2024; accepted 13 August 2024; published 3 September 2024)

A recent experimental study of TbB_4 at a low temperature using resonant x-ray Bragg diffraction implies a magnetic symmetry not found in any other rare-earth tetraboride. The evidence for this assertion is a change in the intensity of a TbB_4 Bragg spot on reversing the handedness (chirality) of the primary x-ray beam [R. Misawa, K. Arakawa, T. Yoshioka, H. Ueda, F. Iga, K. Tamasaku, Y. Tanaka, and T. Kimura, Phys. Rev. B **108**, 134433 (2023)]. It reveals a magnetic chiral signature in TbB_4 that is forbidden in phases of rare-earth tetraborides known to date, as the previous magnetic symmetries are parity-time (PT) symmetric with anti-inversion present in the magnetic crystal class. Misawa *et al.* appeal to a PT-symmetric diffraction pattern to interpret their interesting diffraction patterns. In addition to the use of symmetry that does not permit a chiral signature, calculated patterns impose cylindrical symmetry on Tb sites with no justification. We review magnetic symmetries for TbB_4 consistent with a published neutron powder diffraction pattern and susceptibility measurements. On the basis of this information, noncollinear antiferromagnetic order exists below a temperature ≈ 44 K with no ferromagnetic component. Our symmetry-informed patterns encapsulate Tb electronic degrees of freedom in terms of multipoles consistent with established sum rules for dichroic signals. The investigated symmetry templates are noncentrosymmetric, noncollinear antiferromagnetic constructions with propagation vector $\mathbf{k} = (0, 0, 0)$. An inferred chiral signature for a parity-even absorption event has an interesting composition. There is the anticipated product of Tb axial dipoles and chargelike quadrupoles (from Templeton-Templeton scattering). Beyond this contribution, though, symmetry allows a product of dipoles in the chiral signature. A predicted change in the intensity of a Bragg spot with rotation of the crystal about the reflection vector (an azimuthal angle scan) can be tested in future experiments. Likewise contributions to Bragg diffraction patterns from Tb anapoles and higher-order Dirac multipoles.

DOI: 10.1103/PhysRevB.110.104405

I. INTRODUCTION

Rare-earth borides display a raft of interesting electronic properties, including superconductivity and frustrated magnetism [1]. Tetraborides adopt a tetragonal structure and develop collinear or noncollinear antiferromagnetic orders at low temperatures. Terbium tetraboride, of interest here, displays two phase transitions [2]. Neutron powder diffraction patterns for TbB_4 are consistent with noncollinear antiferromagnetic order below a temperature ≈ 44 K [3]. This type of magnetic order persists beyond a second transition at ≈ 24 K, where terbium dipoles tilt toward the *a* or *b* axes. Magnetic susceptibility measurements rule against a ferromagnetic component [2], and, reassuringly, there is no trace of it in neutron powder diffraction patterns [3]. Magnetic structures present magnetoelectric and concomitant parity-time (PT) symmetry [4].

A new magnetic symmetry of TbB_4 can be inferred from a Bragg diffraction pattern measured by resonant x-ray diffraction with a sample temperature ≈ 30 K, and it is the principal subject of the present paper. A key feature of the pattern reported by Misawa *et al.* [5] is found in their Fig. 4(e). It shows that the intensity of the (3, 0, 0) space-group forbidden Bragg spot changes on reversing the chirality of the primary x rays, from right-handed to left-handed circular polarization, say. Such signatures may be present when magnetic and charge contributions to a diffraction amplitude are separated by a 90° phase shift. Notably, it is forbidden by anti-inversion ($\overline{1}'$) in PT-symmetry. For example, magnetoelectric compounds GdB_4 (magnetic crystal class $4/m'm'm'$), CuMnAs ($m'mm$), and $Cu_2(MoO_4)(SeO_3)$ ($2'/m$) do not present chiral signatures [4,6–8].

The measured chiral signature Fig. 4(e) in Misawa *et al.* [5] rules against the magnetic symmetry for a sample temperature ≈ 30 K depicted in their Fig. 1(a), since the symmetry elements of magnetic crystal class $4/m'm'm'$ include anti-inversion ($\overline{1}'$). An appropriate magnetic symmetry for the new phase of TbB_4 must also account for the intensity of a space-group forbidden Bragg spot displayed in Fig. 3 [5] as a function of the rotation about the reflection vector (an azimuthal angle scan).

Published by the American Physical Society under the terms of the Creative Commons Attribution 4.0 International license. Further distribution of this work must maintain attribution to the author(s) and the published article's title, journal citation, and DOI.

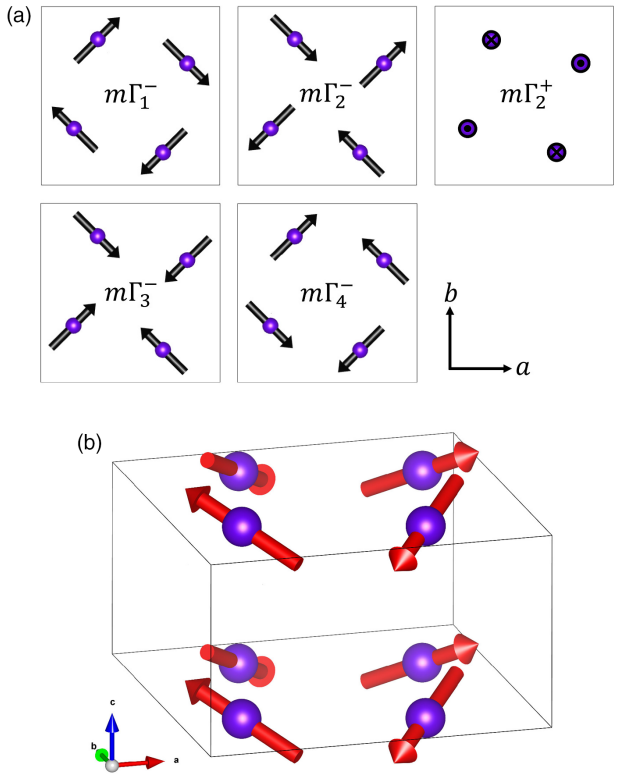

FIG. 1. Panel (a); Five irreps used in the construction of four tetragonal templates defined and discussed in Sec. II. Two templates (i) $m\Gamma_2^+ \oplus m\Gamma_1^-(P\bar{4}'2_{1m'}$, no. 113.270, magnetic crystal class $\bar{4}'2m')$ and $m\Gamma_2^+ \oplus m\Gamma_2^-$ (no. 90.97, $422')$ match diffraction patterns for TbB_4 [5]. Panel (b); Depiction of axial dipoles with magnetic symmetry no. 113.270.

We successfully interpret observations on TbB_4 reported by Misawa *et al.* [5] with symmetry informed Bragg diffraction patterns. To this end, we use a theory of resonant x-ray Bragg diffraction derived with standard Racah algebra for atomic multipoles [6,9,10]. The theory is compatible with tried and tested sum rules in dichroic signals [11–13]. This desirable attribute is not fully realized in a phenomenological theory used by Misawa *et al.* that contains free parameters and a constraint to cylindrical Tb site symmetry [14–16]; see footnote 9 in Ref. [14]. In consequence, diffraction amplitudes are not guaranteed to be compatible with the full magnetic symmetry. Returning to our elected theory, electronic multipoles inferred from experimental data supplied by Misawa *et al.* [5] are listed in Table I. They can be confronted with estimates using an atomic wave function for the resonant ion [13,17,18], or simulations of electronic structure [19–21].

II. TEMPLATE SELECTION

The parent structure of TbB_4 is no. 127 (crystal class $4/mmm$) with Tb in sites $4g$. Suitable templates exclude a ferromagnetic moment [2,3]. For a second-order phase transition at T_N, there is just one template that does not contain anti-inversion, namely, no. 127.391 (BNS [22], $4'/mmm')$, which transforms as irreducible representation (irrep) $m\Gamma_2^+$. It represents an antiferromagnetic structure with Tb axial dipoles aligned along the crystal c axis. With dipoles aligned in this manner it is no surprise that the diffraction pattern for no. 127.391 alone does not match diffraction patterns supplied by Misawa *et al.* [5]. We therefore consider linear combinations of irreps, but in this case the magnetic transition must be first order. Admixing two irreps (more irreps make the search intractable) gives five templates that do not contain anti-inversion. They are no. 117.302 (magnetic crystal class $\bar{4}'m2')$, no. 113.270 $(\bar{4}'2m')$, polar no. 100.174, $(4'mm')$, Sohncke-type no. 90.97 $(422'$ [23]), and no. 26.66 $(422')$, associated with direct sums of six irreps, namely, $m\Gamma_2^+ \oplus m\Gamma_3^-$, $m\Gamma_2^+ \oplus m\Gamma_1^-$, $m\Gamma_2^+ \oplus m\Gamma_4^-$, $m\Gamma_2^+ \oplus m\Gamma_2^-$, and $m\Gamma_2^+ \oplus m\Gamma_5^-$, respectively. We note that all templates include a $m\Gamma_2^+$ mode. The reflection condition $(h, 0, 0)$ with $h = 2n$ or equivalent is not met by orthorhombic no. 26.66. The remaining four tetragonal templates are noncentrosymmetric and describe antiferromagnetic noncollinear motifs of Tb dipoles with a propagation vector $\mathbf{k} = (0, 0, 0)$. Symmetry adapted modes of magnetic dipoles therein are depicted in Fig. 1(a) for the five irreps ultimately required (Γ_5^- in $Pmc2_1$ is absent). Templates $m\Gamma_2^+ \oplus m\Gamma_1^-$ (no. 113.270, $\bar{4}'2m')$ and $m\Gamma_2^+ \oplus m\Gamma_2^-$ [Sohncke-type (chiral) no. 90.97, $422'$] are found to match all aspects of the published x-ray diffraction patterns [5]. Corresponding diffraction amplitudes are presented in Sec. IV. The remaining templates $m\Gamma_2^+ \oplus m\Gamma_3^-$ (no. 117.302, $\bar{4}'m2')$ and $m\Gamma_2^+ \oplus m\Gamma_4^-$ (no. 100.174, $4'mm')$ are shown to fail with regard to the required chiral signature.

It is likely useful to review the PT-symmetric magnetic structure cited by Misawa *et al.* and rejected by us [5]. The magnetic symmetry depicted in their Fig. 1(a) for the higher temperature structure that brackets temperatures 24 and 44 K is a single symmetry adapted mode that transforms by the single irrep $m\Gamma_1^-$. The respective magnetic symmetry is no. 127.395 $(4/m'm'm')$. The magnetic symmetry depicted in their Fig. 1(b) for the low temperature symmetry (temperature < 24 K) is a linear combination of two symmetry adapted modes. One of the two modes is the same as that cited for the above phase observed at a higher temperature. The second mode if appearing by itself presents magnetic symmetry no. 127.392 $(4'/m'm'm)$. The linear combination drawn in Fig. 1(b) in Ref. [5] lowers symmetry to orthorhombic no. 55.359 $(m'm'm')$.

TABLE I. Multipoles for the magnetically ordered phase of TbB_4 (30 K) inferred from experimental data depicted in Fig. 3 [5]. Equation (4) is intensity in the rotated channel of polarization $|(\pi'\sigma)|^2$ for template (i) (no. 113.270). A fit to the displayed data as a function of the azimuthal angle ψ is depicted in blue. Corresponding multipoles are listed here as a function of the axial dipole $\langle T^1_a \rangle$ (arbitrary units). It has a maximum value $\langle T^1_a \rangle = 1.77$ when $\langle T^2_{+2} \rangle'' = 0$.

$\langle T^1_a \rangle$	$\langle T^1_c \rangle$	$\langle T^2_{+1} \rangle'$	$\langle T^2_{+2} \rangle''$
1.7	1.08	0.34	0.13
1.5	0.99	0.66	0.34
1.3	0.88	0.85	0.46
1.1	0.77	0.98	0.55
0.9	0.65	1.08	0.62
0.3	0.30	1.23	0.75

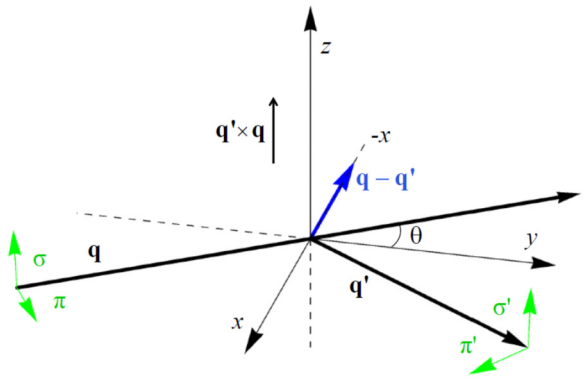

FIG. 2. Primary (σ, π) and secondary (σ', π') states of x-ray polarization. Corresponding photon wave vectors $\mathbf{q}$ and $\mathbf{q}'$ subtend an angle 2θ. Crystal vectors and the depicted Cartesian (x, y, z) coincide in the nominal setting of the crystal. An azimuthal angle ψ used in the main text measures rotation of the crystal about the reflection vector $\kappa = \mathbf{q} - \mathbf{q}'$. We adopt an origin $\psi = 0$ chosen by Misawa *et al.* [5]. The sense of rotation is counterclockwise when viewed down the reflection vector, i.e., the vector $x = z = 0$, $y = 1$ becomes $(0, 0, -1)$ for $\psi = 90°$.

III. RESONANT X-RAY DIFFRACTION

Tuning the energy of x rays to an atomic resonance has two obvious benefits in diffraction experiments [16,24]. In the first place, there is a welcome enhancement of Bragg spot intensities and, secondly, spots are element specific. States of x-ray polarization, Bragg angle θ, and the plane of scattering are shown in Fig. 2. A conventional labeling of linear photon polarization states places $\sigma = (0, 0, 1)$ and $\pi = (\cos(\theta), \sin(\theta), 0)$ perpendicular and parallel to the plane of scattering, respectively [6]. Secondary states $\sigma' = \sigma$ and $\pi' = (\cos(\theta), -\sin(\theta), 0)$. The x-ray scattering length in the unrotated channel of polarization $\sigma \to \sigma'$, say, is modeled by $(\sigma'\sigma)/D(E)$. In this instance, the resonant denominator is replaced by a sharp oscillator $D(E) = \{[E - \Delta + i\Gamma/2]/\Delta\}$ with the x-ray energy E in the near vicinity of an atomic resonance Δ of total width Γ, namely, $E \approx \Delta$ and $\Gamma << \Delta$. The cited energy-integrated scattering amplitude $(\sigma'\sigma)$, one of four amplitudes, is studied using standard tools and methods from atomic physics and crystallography. In the first place, a vast spectrum of virtual intermediate states makes the x-ray scattering length extremely complicated [13]. It can be truncated following closely steps in celebrated studies by Judd and Ofelt of optical absorption intensities of rare-earth ions [13,25–28]. An intermediate level of truncation used here reproduces sum rules for axial dichroic signals created by electric dipole–electric dipole ($E1$-$E1$) or electric quadrupole–electric quadrupole ($E2$-$E2$) absorption events [6,13]. The attendant calculation presented in Ref. [28] and Sec. 5.2 in Ref. [6] is lengthy and demanding. Here, we implement universal expressions for scattering amplitudes and abbreviate notation using $(\sigma'\sigma) \equiv F_{\sigma'\sigma}$, etc., for amplitudes listed by Scagnoli and Lovesey, Appendix C in Ref. [10]. A similar analysis exists for polar absorption events such as $E1$-$E2$ (Appendix D in Ref. [10]), and $E1$-$M1$ where $M1$ is the magnetic moment [29,30]. Here, we interpret Bragg spots observed by Misawa *et al.* [5] with the x-ray energy tuned to the terbium L_3 edge ($E \approx 7.5175$ keV) that accesses $E1$ ($2p \to 5d$) and $E2$ ($2p \to 4f$) absorption events.

In our adopted description of electronic degrees of freedom, Tb ions are assigned spherical multipoles $\langle \mathrm{O}^{\mathrm{K}}_{\mathrm{Q}} \rangle$ of integer rank K with projections Q. Angular brackets denote the time average, or expectation value, of the enclosed spherical tensor operator. A unit-cell electronic structure factor $\Psi^{\mathrm{K}}_{\mathrm{Q}}$ is constructed from all symmetry operations in the chosen space group [22]. Cartesian and spherical components $Q = 0, \pm 1$ of a vector $\mathbf{n} = (\xi, \eta, \zeta)$ are related by $\xi = (n_{-1} - n_{+1})/\sqrt{2}$, $\eta = i(n_{-1} + n_{+1})/\sqrt{2}$, $\zeta = n_0$. A complex conjugate of a multipole is defined as $\langle \mathrm{O}^{\mathrm{K}}_{\mathrm{Q}} \rangle^* = (-1)^{\mathrm{Q}} \langle \mathrm{O}^{\mathrm{K}}_{-\mathrm{Q}} \rangle$, meaning the diagonal multipole $\langle \mathrm{O}^{\mathrm{K}}_{0} \rangle$ is purely real. The phase convention for real and imaginary parts labeled by single and double primes is $\langle \mathrm{O}^{\mathrm{K}}_{\mathrm{Q}} \rangle = [\langle \mathrm{O}^{\mathrm{K}}_{\mathrm{Q}} \rangle' + i \langle \mathrm{O}^{\mathrm{K}}_{\mathrm{Q}} \rangle'']$. Whereupon Cartesian dipoles are $\langle \mathrm{O}^{1}{}_{\xi} \rangle = -\sqrt{2} \langle \mathrm{O}^{1}{}_{+1} \rangle'$ and $\langle \mathrm{O}^{1}{}_{\eta} \rangle = -\sqrt{2} \langle \mathrm{O}^{1}{}_{+1} \rangle''$.

Axial (parity even) multipoles denoted $\langle \mathbf{T}^{\mathrm{K}} \rangle$ possess a time signature $(-1)^{\mathrm{K}}$. They can contribute to diffraction enhanced by $E1$-$E1$ or $E2$-$E2$ absorption events. Bragg spots enhanced by an $E1$-$E1$ event are often dominant contributions to a diffraction pattern [15,16,24]. All multipoles are functions of the quantum numbers that define the core state of photoejected electrons. The dependence on quantum numbers manifests itself in so-called sum rules that relate $\langle \mathbf{O}^{\mathrm{K}} \rangle$ measured at L_2 and L_3 edges, for example [6,11–13]. Sum rules Eqs. (A5) and (A6) for the axial dipole $\langle \mathbf{T}^{1} \rangle$ present the orbital angular momentum $\langle \mathbf{L} \rangle$ in the valence state. Dirac atomic multipoles $\langle \mathbf{G}^{\mathrm{K}} \rangle$ are polar (parity odd) and magnetic (time odd) [6,13]. They are permitted in a magnetic material when the resonant ion occupies an acentric site. Detection of Dirac multipoles requires a probe with matching attributes, of course, which are found in x-ray diffraction enhanced by $E1$-$E2$ or $E1$-$M1$ parity-odd absorption events.

IV. CHIRAL SIGNATURES

Our chiral signature Υ is the change in intensity of a Bragg spot caused by circular polarization in the primary beam of x rays [13,31]:

$$\Upsilon = \{(\sigma'\pi)^*(\sigma'\sigma) + (\pi'\pi)^*(\pi'\sigma)\}''. \tag{1}$$

The four x-ray diffraction amplitudes in Eq. (1) are derived from an electronic structure factor Eq. (A1). Multipoles are presented in a lattice basis that is usually specified relative to the chemical parent lattice of the magnetic symmetry, no. 127 in our case. The basis provides the relation between Miller indices (H_{o}, K_{o}, L_{o}) for the parent lattice and (h, k, l) for the magnetic symmetry.

For future convenience, we attach the label (i) to the tetragonal template no. 113.270. The basis relative to no. 127 is {(1, 0, 0), (0, 1, 0), (0, 0, 1)}. Terbium ions use Wyckoff positions $4e$ with symmetry $m'_{-\mathrm{xy}}$ that imposes the constraint

$$\begin{aligned} \sigma_\pi \sigma_\theta (-1)^{\mathrm{K}} \langle \mathrm{O}^{\mathrm{K}}{}_{-\mathrm{Q}} \rangle &= \sigma_\pi \sigma_\theta (-1)^{\mathrm{K+Q}} \langle \mathrm{O}^{\mathrm{K}}{}_{\mathrm{Q}} \rangle^* \\ &= \exp(i\pi \mathrm{Q}/2) \langle \mathrm{O}^{\mathrm{K}}{}_{\mathrm{Q}} \rangle, \end{aligned} \tag{2}$$

where σ_π and σ_θ are parity and time signatures, respectively. For parity-even absorption events ($E1$-$E1$ and $E2$-$E2$) $\sigma_\pi = +1$ and $\sigma_\theta = (-1)^{\mathrm{K}}$, while $\sigma_\pi = -1$ and $\sigma_\theta = -1$ for

Dirac multipoles [5,13]. Axial magnetic dipole magnitudes along the a and b crystal axes in (i) are identical, i.e., $\langle T^1{}_a\rangle = \langle T^1{}_b\rangle$, and the magnetic symmetry is depicted in Fig. 1(b).

For the space-group forbidden reflection (h, 0, 0) with odd h studied by Misawa *et al.* [5], the electronic structure factor Eq. (A2) satisfies $\Psi^K{}_Q(\mathrm{i}) = 0$ using multipoles with even K, $Q = 0$ and $\sigma_\pi = +1$. In the case of an $E1$-$E1$ event, amplitudes for unrotated polarizations read

$$(\sigma'\sigma)_\mathrm{i} = 0,\ (\pi'\pi)_\mathrm{i} \propto \sin(2\theta)\big[\mathrm{i}\alpha'\cos(\psi)\langle T^1{}_c\rangle + \alpha''\sin(\psi)\,\langle T^1{}_a\rangle\big], \tag{3}$$

and intensity in the rotated channel of polarization reads

$$|(\pi'\sigma)_\mathrm{i}|^2 \propto \cos^2(\theta)\Big[\big\{\alpha''\cos(\psi)\langle T^1{}_\mathrm{a}\rangle - \sqrt{2}\alpha'\sin(\psi)\langle T^2{}_{+2}\rangle''\big\}^2 + \big\{\alpha'\sin(\psi)\langle T^1{}_\mathrm{c}\rangle + \sqrt{2}\alpha''\cos(\psi)\langle T^2{}_{+1}\rangle'\big\}^2\Big]. \tag{4}$$

Subscripts a and c on axial dipoles denote cell edges depicted in Fig. 1. A spatial phase factor $\alpha = \exp(i2\pi hx) = (\alpha' + i\alpha'')$ with $x \approx 0.3172$, and $\alpha'/\alpha'' \approx -3.25$ for (3, 0, 0) [3,5]. Unimportant numerical prefactors omitted in the foregoing results, and those that follow, explain the use of a proportionality sign. The corresponding chiral signature is

$$\Upsilon(\mathrm{i}) \propto \cos(\theta)\,\sin(2\theta)\Big[\sqrt{2}\alpha'\alpha''\langle T^1{}_a\rangle\langle T^1{}_c\rangle + \sin(2\psi)\big\{\alpha''^2\langle T^1{}_a\rangle\langle T^2{}_{+1}\rangle' - \alpha'^2\langle T^1{}_c\rangle\langle T^2{}_{+2}\rangle''\big\}\Big]. \tag{5}$$

Crystal axes (a, b, c) and photon axes (x, y, z) in Fig. 2 are correctly aligned for an azimuthal origin $\psi = 0$. The chiral signature $\Upsilon(\mathrm{i})$ is proportional to $[\langle T^1_a\rangle\langle T^1_c\rangle]$ at $\psi = -90^\circ$, and a nonzero signature at this azimuth accords with the measured diffraction pattern [5]. Likewise for intensity in the rotated channel of polarization as a function of ψ reproduced in Fig. 3. The chiral signature $\Upsilon(90.97)$ is the same as Eq. (5) apart from a change in the sign that accompanies α'^2. Furthermore, intensity in the rotated channel for no. 90.97 is the same as Eq. (4) after a change in the sign with $\langle T^2_{+2}\rangle''$. Hence, template no. 90.97 may also account for experimental diffraction intensities [5].

Equations (4) and (5) for intensity in the rotated channel of polarization and the chiral signature, respectively, are faithful representations of magnetic symmetries no. 90.97 and no. 113.270. Whereas, Eqs. (9) and (12) presented by Mikawa *et al.* are not faithful representations of magnetic symmetry [5]. More specifically, they do not represent the single irrep $m\Gamma_1^-$ (magnetic crystal class $4/m'm'm'$) of the magnetic structure depicted in their Fig. 1(a). Instead, the equations presented by Mikawa *et al.* are products of an abbreviated theory of resonant x-ray diffraction [14] written in terms of some arbitrary parameters. Hence, there is no merit to the chiral signature Eq. (12) in Ref. [5] that appears to be proportional to a product of an axial magnetic dipole and a chargelike quadrupole.

Estimates of the four multipoles in $|(\pi'\sigma)_\mathrm{i}|^2$ in the magnetically ordered phase (30 K) of TbB_4 are inferred from a fit to experimental data [5]. To this end, we parametrize Eq. (4),

$$[u\cos(\psi)]^2 + [v^2 + w^2]\sin^2(\psi) - uw\sin(2\psi),$$

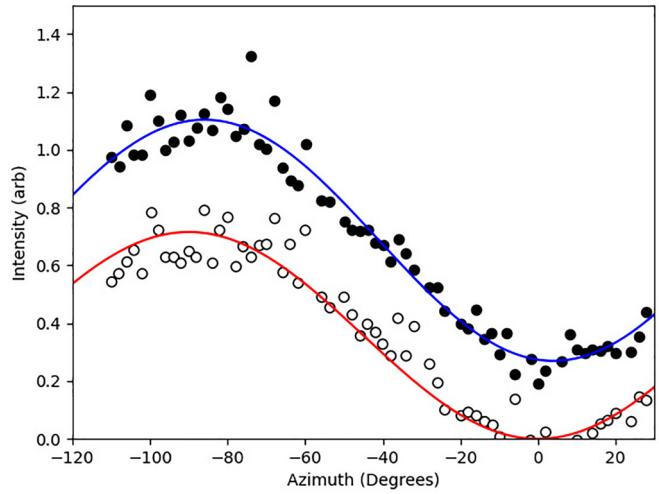

FIG. 3. Integrated intensity as a function of azimuthal angle ψ for template (i) with magnetic symmetry no. 113.270. Solid curves are generated using Eq. (4) for intensity in the rotated channel of polarization $|(\pi'\sigma)_\mathrm{i}|^2$ and the space-group forbidden reflection (3, 0, 0). Sample temperatures 30 K (magnetically ordered phase) and 60 K (paramagnetic) are labeled blue and red, respectively. Experimental data for TbB_4 are extracted from Misawa *et al.* (solid points 30 K, open points 60 K) [5].

and deduce $u \approx 0.52$, $v \approx 1.04$, and $w \approx 0.11$ that generate the blue curve in Fig. 3. Table I contains the relative magnitudes of corresponding multipoles as a function of $\langle T^1{}_a\rangle$ (arbitrary units). Notable features include similar magnitudes for $\langle T^1{}_a\rangle$ and $\langle T^1{}_c\rangle$, and an inverse relation between the magnitudes of dipoles and quadrupoles. In so far as Eq. (4) is relevant for the paramagnetic phase (60 K), the red curve in Fig. 3 is generated with $\langle T^2{}_{+2}\rangle'' \approx 0.63$, and $\langle T^1{}_a\rangle = \langle T^1{}_c\rangle = \langle T^2{}_{+1}\rangle' = 0$. While null values for dipoles are required in the paramagnetic phase, an implied large change in quadrupoles at the magnetic phase transition suggests significant alterations to material properties.

Returning to Sohncke-type magnetic symmetry no. 90.97 [enantiomorphous (chiral) crystal class $4'22'$], Tb ions use Wyckoff positions $4e$ and electronic structure factors $\Psi^K{}_Q(\mathrm{i}) = \Psi^K{}_Q(113.270)$ in Eq. (A2) and $\Psi^K{}_Q(90.97)$ are formally identical. However, site symmetries are not the same with $2'_{xy}$ for no. 90.97 and the constraint by $\exp(-i\pi Q/2)\langle \mathrm{O}^K_Q\rangle = \sigma_\theta(-1)^K\langle \mathrm{O}^K_{-Q}\rangle$. Inversion, mirror, improper rotations, and glide symmetries are absent in Sohncke lattices [23]. A neutral screw axis 2_1 in $P42_12$ is achiral while the atomic structure around the axis is chiral. Of the 65 Sohncke lattices primitive ones are chiral and centred ones are not. Orthorhombic and lower symmetry lattices do not contain one of 11 enantiomorphous pairs and the related space groups are achiral.

Moving on, the tetragonal polar template $m\Gamma_2^+ \oplus m\Gamma_4^-$ (no. 100.174), hereafter labeled (ii), possesses a basis {(1, 0, 0), (0, 1, 0), (0, 0, 1)} relative to the parent no. 127, i.e., the same basis as for template (i). Terbium ions occupy Wyckoff positions $4c$, the constraint Eq. (2) applies, $\langle T^1{}_a\rangle = \langle T^1{}_b\rangle$, and the magnetic symmetry is depicted in Fig. 1(b). For an

$E1$-$E1$ event and a reflection vector $(h, 0, 0)$ with odd h,

$$
\begin{aligned}
(\sigma'\sigma)_{\rm ii} &\propto i\alpha'' \sin(2\psi)\langle T^2{}_{+1}\rangle', \\
(\pi'\pi)_{\rm ii} &\propto i\big[\sin(2\theta)\alpha' \cos(\psi)\langle T^1{}_c\rangle \\
&\quad + \sqrt{2}\sin^2(\theta)\alpha'' \sin(2\psi)\,\langle T^2{}_{+1}\rangle'\big], \\
|(\pi'\sigma)_{\rm ii}|^2 &\propto \big[\big\{\sqrt{2}\sin(\theta)\alpha'' \cos(2\psi)\langle T^2{}_{+1}\rangle' \\
&\quad - \cos(\theta)\alpha' \sin(\psi)\langle T^1{}_c\rangle\big\}^2 \\
&\quad + \big\{\sqrt{2}\cos(\theta)\alpha' \sin(\psi)\langle T^2{}_{+2}\rangle'' \\
&\quad - \alpha'' \sin(\theta)\langle T^1{}_a\rangle\big\}^2\big]. \qquad (6)
\end{aligned}
$$

In contrast to (i), diffraction is allowed in the unrotated channel $(\sigma'\sigma)_{\rm ii}$. Our result for the chiral signature is

$$
\begin{aligned}
\Upsilon(\text{ii}) &\propto \cos(\theta)\cos(\psi)\big[\sin(2\theta)\sin(\psi)\big\{\alpha'^2\langle T^1{}_c\rangle\langle T^2{}_{+2}\rangle'' \\
&\quad - \alpha''^2\langle T^1{}_a\rangle\langle T^2{}_{+1}\rangle'\big\} \\
&\quad + \sqrt{2}\alpha'\alpha''\big\{2(\cos(\theta)\sin(\psi))^2\langle T^2{}_{+1}\rangle'\langle T^2{}_{+2}\rangle'' \\
&\quad - \sin^2(\theta)\langle T^1{}_a\rangle\langle T^1{}_c\rangle\big\}\big]. \qquad (7)
\end{aligned}
$$

The c axis is normal to the plane of scattering in Fig. 3 at the start of an azimuthal angle scan, the setting used by Misawa *et al.* [5]. Notably, Υ(ii) is proportional to $\cos(\psi)$ and zero for $\psi = -90°$. The result conflicts with supplied diffraction patterns, while chiral signatures for templates no. 113.270 and no. 90.97 do not [5].

Use of magnetic symmetry no. 117.302 as a template for magnetic TbB_4 is not supported by diffraction patterns. Its basis is $\{(0, 1, 0), (-1, 0, 0), (0, 0, 1)\}$ relative to no. 127. Terbium ions are in Wyckoff positions $4g$ with symmetry $2'_{\rm xy}$. The electronic structure factor is formally identical to Eq. (A2) with an explicit dependence on the parity of electronic multipoles, but the Tb site symmetry is not the same as that for (ii). However, $\Upsilon(117.302)$ is zero for $\psi = -90°$ like Υ(ii). In consequence, chiral signatures $\Upsilon(100.174)$ and $\Upsilon(117.302)$ fail to represent available diffraction patterns [5].

V. DIRAC MULTIPOLES

An anapole (Dirac dipole, $\sigma_\pi\sigma_\theta = +1$) depicted in Fig. 4 diffracts x rays in resonant scattering enhanced by a parity-odd electric dipole-electric quadrupole ($E1$-$E2$) event, for example. [A vector product $(\mathbf{R} \times \mathbf{S})$ where $\mathbf{R}$ and $\mathbf{S}$ are electronic space (time-even and polar) and spin (time-odd and axial) variables, respectively, represents the discrete symmetry of a spin anapole.] Experimental results for Dirac multipoles in V_2O_3 and CuO have been published together with successful interpretations [13,32,33]. In the case of TbB_4 available Tb resonance events include L_3-$2p \rightarrow 5d$ and $2p \rightarrow 4f$ for $E1$ and $E2$—and M_5—$2d \rightarrow 4f$ and $2d \rightarrow 5d$ for $E1$ and $E2$. Diffraction illuminates Dirac multipoles with ranks $K = 1, 2, 3$. Energies of $E1$-$E1$ and $E1 - E2$ resonances are expected to be different.

We examine the information available for the polar template (ii) using an $E1$-$E2$ absorption event. Terbium ions in (ii) support polar multipoles ($\sigma_\pi\sigma_\theta = -1$) at all temperatures, of course. Dirac multipoles ($\langle \mathbf{G}^{\rm K}\rangle$ with $\sigma_\pi\sigma_\theta = +1$) are also a manifestation of the polar structure and epitomize the low

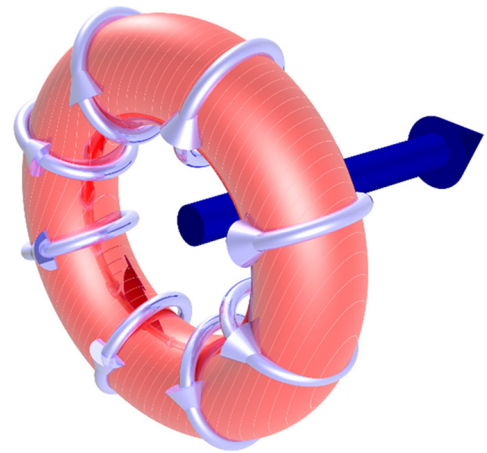

FIG. 4. Depiction of a Dirac dipole (an anapole) created by Scagnoli [33].

temperature magnetic phase. Anapoles in template (ii) satisfy $\langle G^1{}_a\rangle = -\langle G^1{}_b\rangle$ according to Eq. (2). Diffraction amplitudes are derived from Eq. (A3) using expressions in Appendix D of Ref. [10]. Intensity in the rotated channel for $(h, 0, 0)$ with odd h is predicted to be

$$
\begin{aligned}
|(\pi'\sigma)|^2 &\propto \big[\big\{\alpha'\langle G^2{}_0\rangle[(\cos(\theta)\cos(\psi))^2 - \sin^2(\theta)]\big\}^2 \\
&\quad + (2/15)\big\{\sin(2\theta)\alpha'' \sin(\psi)\big[3\langle G^1{}_{+1}\rangle' + 2\sqrt{5}\langle G^2{}_{+1}\rangle' \\
&\quad + (4 - 15\cos^2(\psi))\langle G^3{}_{+1}\rangle' \\
&\quad + \sqrt{15}\cos^2(\psi)\langle G^3{}_{+3}\rangle'\big]\big\}^2\big]. \qquad (8)
\end{aligned}
$$

As with an $E1$-$E1$ absorption event, the chiral signature is zero for $\psi = -90°$. This finding follows from the $E1 - E2$ result:

$$
\begin{aligned}
\Upsilon(\text{ii}) &\propto \alpha'\alpha''\langle G^2{}_0\rangle \cos(\theta)\cos(\psi) \\
&\quad \times \big[(\cos(\theta)\cos(\psi))^2 - \sin^2(\theta)\big] \\
&\quad \times \big[-\sin^2(\theta)\langle G^1{}_{+1}\rangle' + (2/3)\sqrt{5}\cos(2\theta)\,\langle G^2{}_{+1}\rangle' \\
&\quad + (1/12)\{(4 + \cos^2(\theta))(11 - 15\cos^2(\psi)) - 1\}\langle G^3{}_{+1}\rangle' \\
&\quad - (1/4)\sqrt{(5/3)}\{(\cos(\theta)\sin(\psi))^2 + 1\}\langle G^3{}_{+3}\rangle'\big]. \qquad (9)
\end{aligned}
$$

Bragg spots $(h, 0, 0)$ with odd h reveal an anapole along the crystal a axis, a quadrupole ($K = 2$), and an octupole ($K = 3$).

VI. CONCLUSIONS AND DISCUSSION

In summary, we confront four templates of magnetic symmetry designed for terbium tetraboride with limited Bragg diffraction data [5]. Designs descend from the parent structure of TbB_4 and exclude a ferromagnetic component on the grounds of published susceptibility data [2]. Two of the templates match published resonant x-ray diffraction patterns on two counts [5]. First, we have a chiral signature that measures the change to the intensity of a space-group forbidden magnetic Bragg spot brought about by reversing the chirality of the primary x rays, from right-handed to left-handed circular polarization, say. Second, we have a change

in intensity with rotation of the crystal about the reflection vector, usually called an azimuthal angle scan. Notably, a nonzero chiral signature relies on the product of two axial dipoles. Conventional thinking about the signature is in terms of products of a magnetic dipole and a chargelike quadrupole from Templeton-Templeton scattering. Indeed, such a result is exploited by Misawa *et al.* without due regard for symmetry constraints; see Eq. (12) in Ref. [5]. To reiterate, the measured chiral signature—the (3, 0, 0) Bragg spot supplied in Fig. 4(e) in Misawa *et al.* [5]—rules against a PT-symmetric magnetic structure. The two successful templates have magnetic symmetry $P\bar{4}'2_1m'$ (i, no. 113.270, magnetic crystal class $\bar{4}'2m'$) and $P4'2_12'$ (no. 90.97, $422'$), respectively, with the former symmetry encompassing the previously reported in-plane magnetic structure augmented by an antiferromagnetic mode polarized parallel to the c axis. A polar template $P4'bm'$ (ii, no. 100.174) does not present a chiral signature at the observed azimuthal angle, although it meets success with intensity in the rotated channel of polarization Eq. (6). Diffraction patterns for Dirac multipoles in Sec. V tell us more about template (ii) with a view to future experiments. Continuing in this vein, the prediction is that the unrotated diffraction amplitude for template (i) is zero whereas it can be different from zero for (ii).

An investigation of a ferromagnetic component in the magnetic symmetry with interesting results has used monoclinic $P2_1/c$ (no. 14.75, magnetic crystal class $2/m$). It is centrosymmetric unlike (i) and (ii). The Landau free energy includes $[H + HEE]$, with nonlinear magnetoelectric and piezomagnetic effects allowed. The $P2_1/c$ magnetic symmetry is reached through a linear combination of three symmetry-adapted modes defined with respect to the $P4/mbm$ (no. 127) parent. Two of these modes define orthogonal antiferromagnetic (AFM) and ferromagnetic configurations with magnetic dipoles pointing along a and b (or b and a) axes, respectively. They correspond to magnetic symmetry $Pb'am'$ (orthorhombic no. 55.358, $m'mm'$). The addition of an AFM mode with moment components along the crystal c axis (magnetic symmetry $P4'/mbm'$, no. 127.391, $4'/mmm'$) lowers the symmetry to $P2_1/c$ and noncollinear AFM order. Terbium ions occupy general Wyckoff positions $4e$ that are devoid of symmetry including spatial inversion. The chiral signature $\Upsilon(P2_1/c)$ in Eq. (B1) for reflections $(0,\ k,\ 0)$ with odd Miller index k matches $\Upsilon(i)$ in reproducing the limited diffraction patterns on offer [5].

ACKNOWLEDGMENT

S.W.L. is pleased to acknowledge ongoing intellectual support from Dr. K. S. Knight.

APPENDIX A: ELECTRONIC STRUCTURE FACTORS

Our electronic structure factor [6,13],

$$\Psi^{\mathrm{K}}{}_{\mathrm{Q}} = \big[\exp(i\kappa\cdot\mathbf{d})\langle \mathrm{O}^{\mathrm{K}}{}_{\mathrm{Q}}\rangle_{\mathbf{d}}\big], \tag{A1}$$

delineates a Bragg diffraction pattern for a reflection vector $\boldsymbol{\kappa}$ defined by integer Miller indices (h, k, l). The $\Psi^{\mathrm{K}}{}_{\mathrm{Q}}$ respects all symmetries of the specified magnetic space group [22].

In more detail, Eq. (A1) possesses information about the relevant Wyckoff positions available in the Bilbao table MWYCKPOS for the magnetic symmetry of interest [22]. Site symmetry that might constrain projections Q in the range $-K \leqslant Q \leqslant Q$ of a multipole $\langle \mathrm{O}^{\mathrm{K}}{}_{\mathrm{Q}}\rangle$ is given in the same table. The basis relative to the parent no. 127 for templates (i) and (ii) is the same with cell dimensions $a \approx 7.120$ Å, $b \approx 7.120$ Å, $c \approx 4.042$ Å, and alpha = beta = gamma = 90° [3]. Wyckoff positions in a unit cell are related by operations listed in the table MGENPOS [22]. Taken together, the two tables provide all information required to evaluate Eq. (A1) and, thereafter, diffraction amplitudes [10].

For Wyckoff positions $4e$ in tetragonal $P\bar{4}'2_1m'$ (no. 113.270), the magnetic symmetry labeled (i) in the main text reads

$$\begin{aligned}\Psi^{\mathrm{K}}{}_{\mathrm{Q}}(i) = (-1)^k\langle \mathrm{O}^{\mathrm{K}}{}_{\mathrm{Q}}\rangle\big[\alpha\beta + (\alpha\beta)^*(-1)^{\mathrm{Q}}\big] \\ + (-1)^h\langle \mathrm{O}^{\mathrm{K}}{}_{-\mathrm{Q}}\rangle(-1)^{\mathrm{K}}[\alpha\beta^* + \alpha^*\beta(-1)^{\mathrm{Q}}].\end{aligned} \tag{A2}$$

Spatial phase factors are $\alpha = \exp(i2\pi hx)$ and $\beta = \exp(i2\pi kx)$ with a general coordinate $x \approx 0.3172$ [3]. Turning to Wyckoff positions $4c$ in the polar template $P4'bm'$ (no. 100.174), the corresponding electronic structure factor $\Psi^{\mathrm{K}}{}_{\mathrm{Q}}$ (ii) is similar to Eq. (2). We find

$$\begin{aligned}\Psi^{\mathrm{K}}{}_{\mathrm{Q}}(\mathrm{ii}) = (-1)^k\langle \mathrm{O}^{\mathrm{K}}{}_{\mathrm{Q}}\rangle[\alpha\beta + (\alpha\beta)^*(-1)^{\mathrm{Q}}] \\ + \sigma_\pi(-1)^h\langle \mathrm{O}^{\mathrm{K}}{}_{-\mathrm{Q}}\rangle(-1)^{\mathrm{K+Q}}[\alpha\beta^* + \alpha^*\beta(-1)^{\mathrm{Q}}].\end{aligned} \tag{A3}$$

The general coordinate is again $x \approx 0.3172$, and multipoles $\langle \mathrm{O}^{\mathrm{K}}{}_{\mathrm{Q}}\rangle$ in $\Psi^{\mathrm{K}}{}_{\mathrm{Q}}$ (i) and $\Psi^{\mathrm{K}}{}_{\mathrm{Q}}$ (ii) must satisfy Eq. (1).

The identity $\Psi^{\mathrm{l}}{}_{\mathrm{Q}}(\mathrm{i}) = 0$ obtained with $\kappa = (0,\ 0,\ l)$ is expected, because symmetry in the magnetic crystal class $\bar{4}'2m'$ forbids (bulk) ferromagnetism. Notably, $\Psi^{\mathrm{K}}{}_{\mathrm{Q}}$ (ii) depends on parity via its signature σ_π. The identity for ferromagnetism prevails with $\sigma_\pi = +1$. The Landau free energy of nonpolar templates $P\bar{4}'b2'$, $P\bar{4}'2_1m'$, and $P4'2_12'$ takes the form $[EH + EHH + HEE]$, where E and H represent electric and magnetic fields, respectively. Magnetoelectric and piezomagnetic effects are allowed. The Landau free energy for polar $P4'bm'$ (no. 100.174) possesses a contribution linear in E.

Lastly, for Wyckoff positions $4e$ in monoclinic $P2_1/c$ (no. 14.75) mentioned in Sec. VI and the subject of Appendix B, we have

$$\begin{aligned}\Psi^{\mathrm{K}}{}_{\mathrm{Q}}(P2_1/c) \\ = \langle \mathrm{O}^{\mathrm{K}}{}_{\mathrm{Q}}\rangle\big[\beta\gamma + \sigma_\pi(\beta\gamma)^*\big] + (-1)^{k+l}(-1)^{\mathrm{K+Q}}\langle \mathrm{O}^{\mathrm{K}}{}_{-\mathrm{Q}}\rangle \\ \times [\beta^*\gamma + \sigma_\pi(\beta^*\gamma)^*].\end{aligned} \tag{A4}$$

The basis relative to the parent no. 127 is {(0, 0, 1), (1, 0, 0), (0, 1, 0)} with cell dimensions $a \approx 4.042$ Å, $b \approx 7.120$ Å, $c \approx 7.120$ Å, and alpha = beta = gamma = 90°. The spatial phase factors are $\beta = \exp(i2\pi ky)$ and $\gamma = \exp(i2\pi lz)$ with general coordinates $y \approx 0.3175$ and $z \approx 0.8175$. The result $\Psi^{1}{}_{+1}(P2_1/c) \propto \langle T^{1}{}_{+1}\rangle''$ obtained with $\kappa = (h,\ 0,\ 0)$ confirms that a ferromagnetic component along the tetragonal crystal a axis is permitted.

The axial dipole $\langle \mathbf{T}^1\rangle$ in our elected theory of Bragg diffraction obeys a sum rule announced in the first place for dichroic signals [11,12]. The $E1$-$E1$ sum rule presents the

orbital angular momentum $\langle \mathbf{L} \rangle_l$ in the valence state. Specifically [6],

$$[\langle \mathbf{T}^1 \rangle_- + \langle \mathbf{T}^1 \rangle_+]_{11} = \langle \mathbf{L} \rangle_l [l_c(l_c+1) - 2 - l(l+1)] \times [2\sqrt{2}l(l+1)(2l+1)]^{-1}. \quad \text{(A5)}$$

Here, l and l_c are the valence and core angular momenta, and subscripts $\pm$ denote total core angular momenta ($l_c \pm 1/2$). In consequence, a sum of dipoles at L_2 and L_3 edges satisfies $[\langle \mathbf{T}^1 \rangle_- + \langle \mathbf{T}^1 \rangle_+]_{11} = -\langle \mathbf{L} \rangle_d/(10\sqrt{2})$ on using states $p \rightarrow d$ [17]. The dipole sum rule for an $E2$-$E2$ event is $[\langle \mathbf{T}^1 \rangle_- + \langle \mathbf{T}^1 \rangle_+]_{22} = -\langle \mathbf{L} \rangle_f (1/21)\sqrt{(2/5)}$ on using $p \rightarrow f$ in

$$[\langle \mathbf{T}^1 \rangle_- + \langle \mathbf{T}^1 \rangle_+]_{22} = \langle \mathbf{L} \rangle_l [l_c(l_c+1) - 6 - l(l+1)] \times [2\sqrt{10}l(l+1)(2l+1)]^{-1}. \quad \text{(A6)}$$

APPENDIX B: MONOCLINIC TEMPLATE

The descent in lattice symmetry from tetragonal to monoclinic $P2_1/c$ (no. 14.75) is allowed without a change of origin or unit cell volume. The magnetic crystal class $2/m$ is a subgroup of $4/mmm$. From the electronic structure factor Eq. (A4), an antiferromagnetic motif of Tb axial dipole moments with zero propagation vector $\mathbf{k} = (0, 0, 0)$ can possess components in the tetragonal (bc) plane together with a ferromagnetic component along the a axis. Miller indices for the parent structure (H_o, K_o, L_o) and monoclinic magnetic structure (h, k, l) are related by $h = L_o$, $k = H_o$, $l = K_o$. The $P2_1/c$ chiral signature for reflections $(0, k, 0)$ with odd k is

$$\Upsilon(P2_1/c) \propto (\beta')^2 \cos(\theta) \sin(2\theta) \big[\sin(\psi) \langle T^1{}_b \rangle + \cos(\psi) \langle T^1{}_c \rangle \big] \big[\cos(\psi) \langle T^2{}_{+2} \rangle'' - \sin(\psi) \langle T^2{}_{+1} \rangle'' \big], \quad \text{(B1)}$$

with $\beta' = \cos(2\pi kx)$ [3]. The origin of the azimuthal angle $\psi = 0$ posts the tetragonal c axis normal to the plane of scattering in Fig. 3. Evidently, $\Upsilon(P2_1/c)$ can be different from zero for an azimuthal angle $\psi = -90°$, which matches $\Upsilon(113.270)$ and $\Upsilon(90.97)$ and available diffraction patterns Fig. 4(e) [5]. The result Eq. (B1) is derived from diffraction amplitudes:

$$\begin{aligned} (\sigma'\sigma) &= 0, \\ (\pi'\pi) &\propto -i\beta' \sin(2\theta) \big[\sin(\psi) \langle T^1{}_b \rangle + \cos(\psi) \langle T^1{}_c \rangle \big], \\ (\pi'\sigma) &\propto \beta' \cos(\theta) \big[i \big\{ \sin(\psi) \langle T^1{}_c \rangle - \cos(\psi) \langle T^1{}_b \rangle \big\} \\ &\quad + \sqrt{2} \big\{ \cos(\psi) \langle T^2{}_{+2} \rangle'' - \sin(\psi) \langle T^2{}_{+1} \rangle'' \big\} \big]. \end{aligned} \quad \text{(B2)}$$

Setting $\langle T^2_{+2} \rangle'' \approx 0$ in the intensity $|(\pi'\sigma)|^2$ brings satisfactory agreement with the experimental results. Template (i) and $P2_1/c$ (no. 14.75) do not allow diffraction in the unrotated channel since $(\sigma'\sigma) = 0$ for both magnetic symmetries.

By way of a contrast in magnetic properties based on monoclinic $P2_1/c$, PT-symmetry in $P2'_1/c$ used by $Cu_2(MoO_4)(SeO_3)$ (no. 14.77, $2'/m$) forbids a chiral signature [8]. A piezomagnetic effect and ferromagnetism are forbidden, and the Landau free energy [EH] is compatible with a linear magnetoelectric effect. Orthogonal Cartesian axes (ξ, η, ζ) with unique axis η may frame an electronic structure factor. Regarding diffraction enhanced by an $E1$-$E1$ absorption event, all $(0, 0, 2n+1)$ amplitudes can be different from zero for example. Active axial multipoles are dipoles $\langle T^1{}_\xi \rangle$ and $\langle T^1{}_\zeta \rangle$ in the plane normal to the η axis, and quadrupoles $\langle T^2{}_{+1} \rangle''$ and $\langle T^2{}_{+2} \rangle''$. The latter appears in the unrotated channel with a diffraction amplitude $(\sigma'\sigma) \propto [\sin(2\psi) \langle T^2_{+2} \rangle'']$, while $[\cos(\psi) \langle T^1_\xi \rangle]$ and $[\sin(2\psi) \langle T^2{}_{+2} \rangle'']$ feature in $(\pi'\pi)$.

[1] *Rare-Earth Borides*, edited by D. S. Inosov (Jenny Stanford, Singapore, 2021).

[2] Z. Fisk, M. B. Maple, D. C. Johnston, and L. D. Woolf, Solid State Commun. **39**, 1189 (1981).

[3] T. Matsumura, D. Okuyama, and Y. Murakami, J. Phys. Soc. Jpn. **76**, 015001 (2007).

[4] J. A. Blanco, P. J. Brown, A. Stunault, K. Katsumata, F. Iga, and S. Michimura, Phys. Rev. B. **73**, 212411 (2006).

[5] R. Misawa, K. Arakawa, T. Yoshioka, H. Ueda, F. Iga, K. Tamasaku, Y. Tanaka, and T. Kimura, Phys. Rev. B **108**, 134433 (2023).

[6] S. W. Lovesey, E. Balcar, K. S. Knight, and J. Fernández-Rodríguez, Phys. Rep. **411**, 233 (2005).

[7] S. W. Lovesey, D. D. Khalyavin, and G. van der Laan, Phys. Rev. B **108**, 174437 (2023).

[8] P. Piyawongwatthana, K. Nawa, S. Calder, D. Okuyama, H-C. Wu, and T. J. Sato, Phys. Rev. B **109**, 224420 (2024).

[9] J. Luo, G. T. Trammell, and J. P. Hannon, Phys. Rev. Lett. **71**, 287 (1993).

[10] V. Scagnoli and S. W. Lovesey, Phys. Rev. B **79**, 035111 (2009).

[11] B. T. Thole, P. Carra, F. Sette, and G. van der Laan, Phys. Rev. Lett. **68**, 1943 (1992); P. Carra, B. T. Thole, M. Altarelli, and X. D. Wang, *ibid.* **70**, 694 (1993); P. Carra, H. König, B. T. Thole, and M. Altarelli, Physica B **192**, 182 (1993).

[12] G. van der Laan, *International Tables for Crystallography* (Wiley, New York, 2022), Vol. 1.

[13] S. W. Lovesey and E. Balcar, J. Phys. Soc. Jpn. **82**, 021008 (2013).

[14] J. P. Hannon, G. T. Trammell, M. Blume, and Doon Gibbs, Phys. Rev. Lett. **61**, 1245 (1988); J. P. Hannon, *ibid.* **62**, 2644(E) (1989).

[15] J. Hill and D. McMorrow, Acta. Crystallog. A **52**, 236 (1996).

[16] L. Paolasini, Collection SFN **13**, 03002 (2014).

[17] L. C. Chapon and S. W. Lovesey, J. Phys.: Condens. Matter **23**, 252201 (2011).

[18] S. W. Lovesey, C. Detlefs, and A. Rodríguez-Fernández, J. Phys.: Condens. Matter **24**, 256009 (2012).

[19] Y. Joly, S. P. Collins, Stéphane Grenier, Helio C. N. Tolentino, and Maurizio De Santis, Phys. Rev. B **86**, 220101(R) (2012).

[20] M.-To Suzuki, H. Ikeda, and P. M. Oppeneer, J. Phys. Soc. Jpn. **87**, 041008 (2018).

[21] O. Bunău, A. Y. Ramos, and Y. Joly, The FDMNES code in *International Tables for Crystallography* (Wiley, New York, 2022), Vol. 1.
[22] We use the Belov-Neronova-Smirnova setting of magnetic space groups; see the Bilbao Crystallographic server, http://www.cryst.ehu.es.
[23] G. H. Fecher, J. Kübler, and C. Felser, Materials **15**, 5812 (2022).
[24] C. Vettier, J. Electron Spectroscopy and Related Phenomena **117–118**, 113 (2001).
[25] B. R. Judd, Phys. Rev. **127**, 750 (1962).
[26] G. S. Ofelt, J. Chem. Phys. **37**, 511 (1962).
[27] M. P. Hehlen, M. G. Brik, and Karl W. Krämer, J. Luminescence **136**, 221 (2013).
[28] S. W. Lovesey and E. Balcar, J. Phys.: Condens. Matter **9**, 4237 (1997).
[29] S. W. Lovesey and E. Balcar, J. Phys. Soc. Jpn. **79**, 074707 (2010).
[30] S. W. Lovesey and E. Balcar, J. Phys. Soc. Jpn. **79**, 104702 (2010).
[31] J. Fernández-Rodríguez, S. W. Lovesey, and J. A. Blanco, Phys. Rev. B **77**, 094441 (2008).
[32] J. Fernández-Rodríguez, V. Scagnoli, C. Mazzoli, F. Fabrizi, S. W. Lovesey, J. A. Blanco, D. S. Sivia, K. S. Knight, F. de Bergevin, and L. Paolasini, Phys. Rev. B **81**, 085107 (2010).
[33] V. Scagnoli, U. Staub, Y. Bodenthin, R. A. de Souza, M. García-Fernández, M. Garganourakis, A. T. Boothroyd, D. Prabhakaran, and S. W. Lovesey, Science. **332**, 696 (2011).